The Substrate Import Mechanism of the Human Serotonin Transporter

Matthew C. Chan,[†,⊥] Balaji Selvam,[†,⊥] Heather J. Young,[‡,⊥] Erik Procko,[*,‡,¶] and Diwakar Shukla[*,†,¶,§,‖]

†*Department of Chemical and Biomolecular Engineering, University of Illinois at Urbana-Champaign, Urbana, IL, 61801*

‡*Department of Biochemistry, University of Illinois at Urbana-Champaign, Urbana, IL, 61801*

¶*Center for Biophysics and Quantitative Biology, University of Illinois at Urbana-Champaign, Urbana, IL, 61801*

§*National Center for Supercomputing Applications, University of Illinois, Urbana, IL, 61801*

‖*NIH Center for Macromolecular Modeling and Bioinformatics, University of Illinois at Urbana-Champaign, Urbana, IL, 61801*

⊥*These authors contributed equally.*

E-mail: procko@illinois.edu; diwakar@illinois.edu

Abstract

The serotonin transporter, SERT, initiates the reuptake of extracellular serotonin in the synapse to terminate neurotransmission. Recently, the cryo-EM structures of SERT bound to ibogaine resolved in different states provided the first glimpse of functional conformations at atomistic resolution. However, the conformational dynamics

and structural transitions to various intermediate states are not fully understood. Furthermore, while experimental SERT structures were complexed with drug molecules and inhibitors, the molecular basis of how the physiological substrate, serotonin, is recognized, bound, and transported remains unclear. In this study, we performed microsecond long simulations of the human SERT to investigate the structural dynamics to various intermediate states and elucidated the complete substrate import pathway. Using Markov state models, we characterized a sequential order of conformational driven ion-coupled substrate binding and transport events and calculated the free energy barriers of conformation transitions associated with the import mechanism. We identified a set of crucial residues that recognize the substrate at the extracellular surface of SERT and our biochemical screening results show that mutations causes dramatic reduction in transport function. Our simulations also revealed a third sodium ion binding site coordinated by Glu136 and Glu508 in a buried cavity which helps maintain the conserved fold adjacent to the orthosteric site for transport function. The mutation of these residues results in a complete loss of transport activity. Our study provides novel insights on the molecular basis of dynamics driven ion-substrate recognition and transport of SERT that can serve as a model for other closely related neurotransmitter transporters.

Introduction

The serotonin transporter (SERT) terminates synaptic transmission by catalyzing the reuptake of extracellular serotonin from the synapse. Reuptake is critical for normal serotonergic signaling in the brain with implications on mood, cognition, behavior, and appetite.[1–4] Consequently, improper SERT function is associated with numerous neurological disorders including depression, post-traumatic stress disorder, autism, and bipolar disorder.[5–9] Additionally, SERT is expressed in platelet membranes and regulates blood coagulation throughout the circulatory system.[10,11] Given its medical importance, SERT is a major molecu-

lar target for therapeutic drugs and drugs of abuse.[12,13] Similar to other members of the solute carrier 6 (SLC6) neurotransmitter transporter family, SERT mediated serotonin (5-hydroxytryptamine; 5HT) translocation from the synapse and surrounding area is coupled to favorable ion co-transport of one Na^+, one Cl^-, and export of one K^+ to complete an overall electroneutral cycle.[14–20] Other conduction states and stoichiometries with unclear physiological significance may occur under different conditions.[21–25]

SERT, and the closely related dopamine transporter (DAT) and norepinephrine transporter (NET), belongs to a class of monoamine transporters in the neurotransmitter:sodium symporter (NSS) family. These members share a distinct architecture known as the LeuT fold, which consist of 12 transmembrane (TM) helices, with TM1-5 and TM6-10 forming inverted pentahelical repeats around a pseudo two-fold axis of symmetry.[26,27] Historically, the bacterial NSS homolog leucine transporter (LeuT) from *Aquifex aeolicus* has served as a structural template to study monoamine transporters.[28–32] Crystal structures of LeuT obtained in the outward-facing (OF), occluded (OC), and inward-facing (IF) states have established the NSS transport process by an alternating access mechanism, in which the substrate and ions first access their central binding sites via an open extracellular vestibule, and then are released within the cell through the sequential closure of an extracellular gate and opening of an intracellular exit pathway.[27,33–36] Based on in-depth studies of bacterial transporters, including fluorescence spectroscopy,[37–39] molecular modeling,[40,41] and single molecule imaging,[42] substrate permeation through the NSS family transporters is facilitated by reorientation of helices around the central axis, in particular the movement of TM1a away from the helical bundle to open an intracellular vestibule for substrate release.[33,43,44] Despite low sequence similarity with human NSS transporters, these efforts paved the way for rational drug design for treating various psychiatric disorders.[45–47]

Structural investigations into human NSS transporters have further benefited from the more recent resolution of outward-facing conformations of eukaryotic monoamine transporters *Drosophila* DAT (*d*DAT) and human SERT (*h*SERT).[48–50] The screening and dock-

ing studies using these crystal structures provide the structural basis of antidepressant recognition and inhibition.[51–56] Most recently, cryogenic electron microscopy (cryo-EM) structures of *h*SERT complexed with the psychedelic non-competitive inhibitor ibogaine reveal the occluded and inward-facing states with similar structural arrangements as seen in LeuT.[27,35,57,58] However, given the structural discrepancies between SERT and other NSS structural models, the molecular basis of transitions between the intermediate states remains unknown. Closure of the extracellular vestibule is coordinated by helical motions of TM1b and TM6a where Arg79 and Glu493 are proposed to serve as extracellular gating residues to stabilize the OC and IF states. The helix orientation of TM1b in the SERT OC conformation is closely aligned to that of OF LeuT. Moreover, among the current SERT OF structures, the distance between the guanidinium group of Arg79 and carboxyl of Glu493 varies from 4.4 Å to 7.4 Å, while in the OC and IF states, this distance is 7.2 Å and 4.6 Å, respectively. As a result, the role of these gating residues and their interactions during conformational transitions is unclear. The N-terminal loop preceding TM1a and its interactions with TM6 and TM8 regulates the helix motion of TM1a during substrate release and acts as an intracellular gate.[44,59,60] Hydrogen-deuterium exchange (HDX) experiments have provided an alternative approach to understand the conformational dynamics within the NSS family and have shown that ion-substrate binding facilitates changes in dynamics in TM1a, TM6, and TM7.[28,61–63] Intricate loop dynamics, specifically motions of extracellular loops (EL) 3 and 4 fluctuates significantly during substrate transport.[28,61–63] The combined structural and biochemical studies have provided invaluable insights in the functional mechanism of the NSS family. However, the realistic motions of structural transitions at atomistic resolution are not fully known to understand the conformational driven substrate transport cycle.

In this study, we performed unbiased all-atom molecular dynamics (MD) simulations to obtain a comprehensive understanding of the import mechanism for the physiological substrate serotonin in *h*SERT. Our study shows the key binding and transport events, including substrate interactions at an extracellular allosteric site, neurotransmitter binding within sub-

site B, coordination of three metal ions, and a single symported sodium ion being displaced into the cytosol by the movement of serotonin into the exit pathway. Using a Markov state model (MSM)-based adaptive sampling approach to explore the conformational landscape, we report a sequential order of the ion-substrate binding and transport processes for any NSS family transporter. The free energy conformational landscape plots reveal that structural isomerization from OC to IF is a rate-limiting step for import that is facilitated by the presence of 5HT in the orthosteric site. We identified a third sodium ion binding site in a buried cavity close to the orthosteric site which helps maintain the fold for substrate transport. We determined the key residues that are involved in 5HT recognition, binding, and transport, and validated our predictions using site-directed mutagenesis. Our results provide an in-depth perspective into the molecular recognition and transport of 5HT in SERT and may aid for the development of conformational selective inhibitors for the treatment of psychiatric disorders.

Results

Substrate binding decreases the free energy barrier for SERT conformational transitions to the IF state.

To understand the effects of substrate-induced protein dynamics, the entire import process of 5HT was studied using molecular dynamics (MD) simulations. A Markov state model (MSM)-based adaptive sampling approach was used to explore the entire accessible conformational space.[64–66] Simulations were initiated from the OF crystal structure of *h*SERT (PDB: 5I73) and a total of 130 μs of 5HT-free SERT (referred to as *apo*-SERT) was obtained. Na^+-bound SERT in an OF conformation obtained from *apo*-SERT simulations, with the Na1 and Na2 sites occupied, was used to seed simulations of the 5HT import process (referred to as 5HT-SERT). 100 mM 5HT was added to the simulation box (equivalent to 12 5HT molecules) and a total of 170 μs data were collected. All simulation data were

used to construct an MSM, which parses the simulation data into kinetically relevant states and calculates the transition probabilities between the states (See Methods for additional details). MSM-weighted simulation data were projected onto a coordinate system defined by distances between extracellular and intracellular gating residues (Figure 1).

The conformational landscape plots reveal that despite the absence of 5HT binding, *apo*-SERT may undergo transitions from the OF state to the IF state (Figure 1A). Extracellular gating residues Arg104 (TM1b) and Glu493 (TM10) can separate to 10 Å, enlarging the extracellular entrance tunnel. The equivalent charged residues in the bacterial transporter LeuT have been previously implicated in the gating mechanism.[27,67] The OF states are stable, with a relative free energy of ∼0.5 kcal/mol. The distance between gating residues Arg104-Glu493 decreases to 3 Å and is associated with electrostatic interactions (Figure S1), forming OC conformations that are slightly more stable than the OF state. Closure of the extracellular entrance tunnel as SERT isomerizes from the OF to OC state weakens contacts on the intracellular side of the transporter, creating an energetically accessible pathway towards the IF state. The free energy barrier for transition from the OC-IF state in *apo*-SERT is estimated as ∼3 kcal/mol, which is higher compared to the OF-OC transition (∼2 kcal/mol). Formation of the IF state is associated with breakage of electrostatic interactions between Arg79 (TM1a) and Asp452 (TM8) at the intracellular gate and increased dynamics of the flanking loops (Figure S1). Simulated helical rearrangements involved in opening and closing of the transporter agree with the recent cryo-EM structures[57] and other NSS crystal structures[35,51,53] (Figure S2).

The substrate-present conformational landscape plot exhibits deviations in the relative free energies of conformational states and reduced free energy barriers between states (Figure 1B). Binding of 5HT in the entrance tunnel stabilizes the OF states to a greater extent compared to *apo* simulations. The gating residues form alternative interactions with Gln332 (TM6) and Lys490 (TM10), thereby widening the extracellular vestibule (Figure S1). The diffusion of 5HT to the orthosteric (S1) site via the allosteric (S2) site leads to the closure

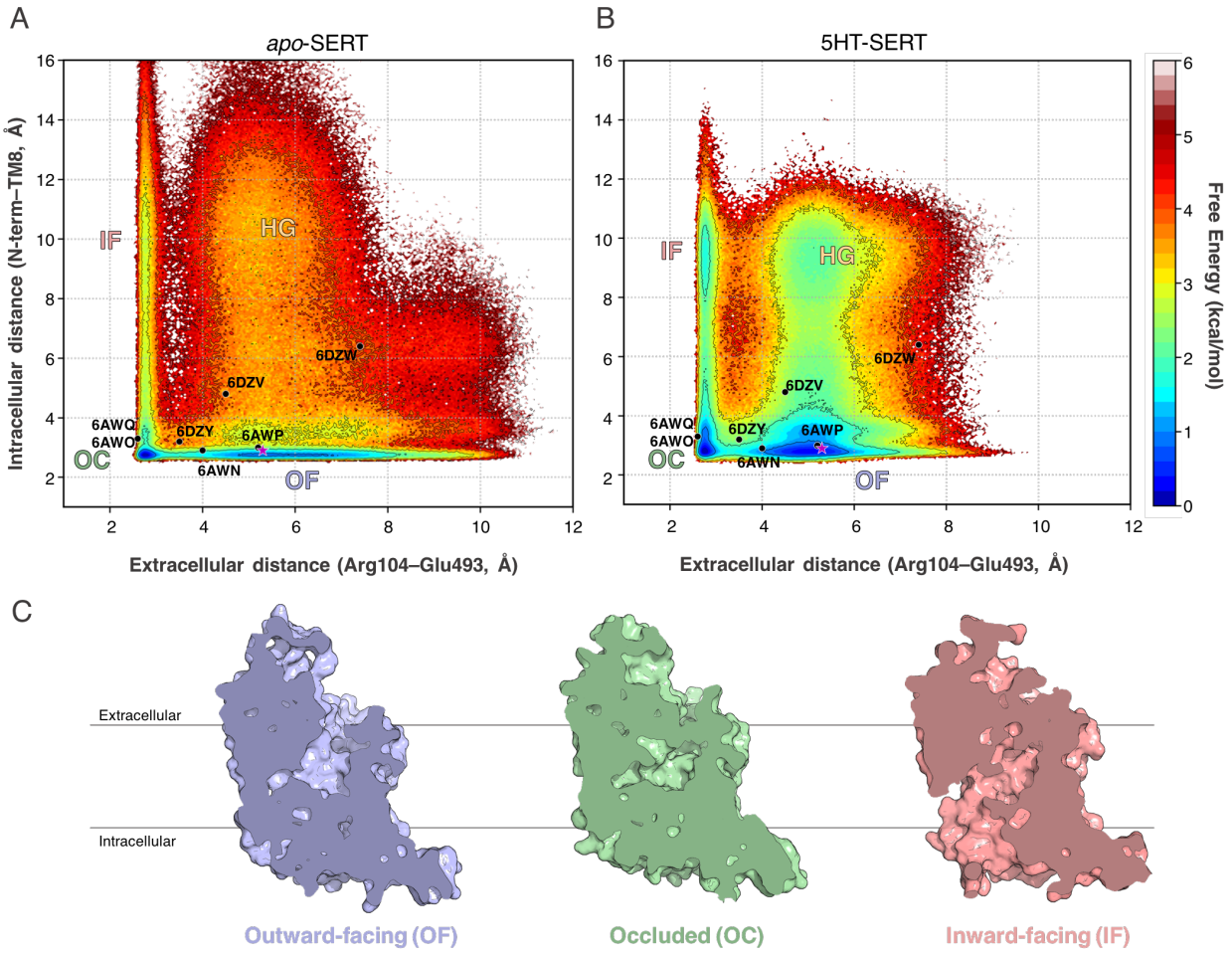

Figure 1: Conformational free energy landscapes of SERT obtained from MD simulations. Relative free energies from MSM-weighted simulation data plotted against the distances between extracellular and intracellular gates for (A) *apo*-SERT and (B) 5HT-SERT. An outward-facing (OF) SERT crystal structure (PDB 5I73, pink star) was used as the starting structure for MD simulations and transitioned to occluded (OC) and inward-facing (IF) states. An hourglass-like (HG) state, in which both gates are open, was also observed. Crystal and cryo-EM structures are plotted on the conformational landscapes in black circles. (C) Cross-sections through SERT conformational states viewed from the membrane plane, shown as surface representations.

of the extracellular cavity to obtain an OC state. The OF-OC transition has a free energy barrier of ∼1.5kcal/mol, similar to *apo*-SERT. The 'downward' movement of 5HT facilitates opening of the intracellular gate and isomerization to the IF state. The free energy barrier for the OC-IF structural transition is estimated as ∼1.5-2 kcal/mol, substantially lower than for *apo*-SERT. The presence of 5HT in the intracellular pathway stabilizes SERT in the IF state, with a relative free energy of ∼1 kcal/mol as compared to ∼3 kcal/mol in *apo*-SERT. We also observed partial OF-IF like conformations, which we have termed as an hourglass-like (HG) state in which both gates are open but constricted at the center (Figure S3C). This state has been observed in other membrane transporters[68] including a disease-associated mutant of DAT,[69–71] but transitions from HG to other intermediate states are restricted as the free energy barriers are high and the physiological relevance of this state in SERT remains elusive.

MD predicted substrate-bound SERT closely matches with experimental observables.

The simulated structures show similar helical orientations at the extracellular and intracellular gates with respect to experimental SERT structures (Figure S2).[35,51,53] The comparison of *apo* and 5HT-SERT data reveal that the structural transitions from OF to OC involve minimal helical movements in TM1b, TM6a, and TM10, while OC to IF transitions show higher fluctuations of intracellular helix tips of TM1a, TM5, and TM7 to facilitate opening of the intracellular vestibule (Figure S2). Large deviations were observed in the opening of the intracellular vestibule of the IF state between the cryo-EM and predicted MD structure. This might reflect the loss of lateral pressure following detergent-extraction; the membrane is anticipated to constrain the extent to which TM1a can move away from the helical bundle. However, our results show that partial opening of the intracellular cavity is sufficient for the substrate transport. Experimental studies of LeuT also indicate that a partially-open IF conformation is suitable for substrate transport.[32]

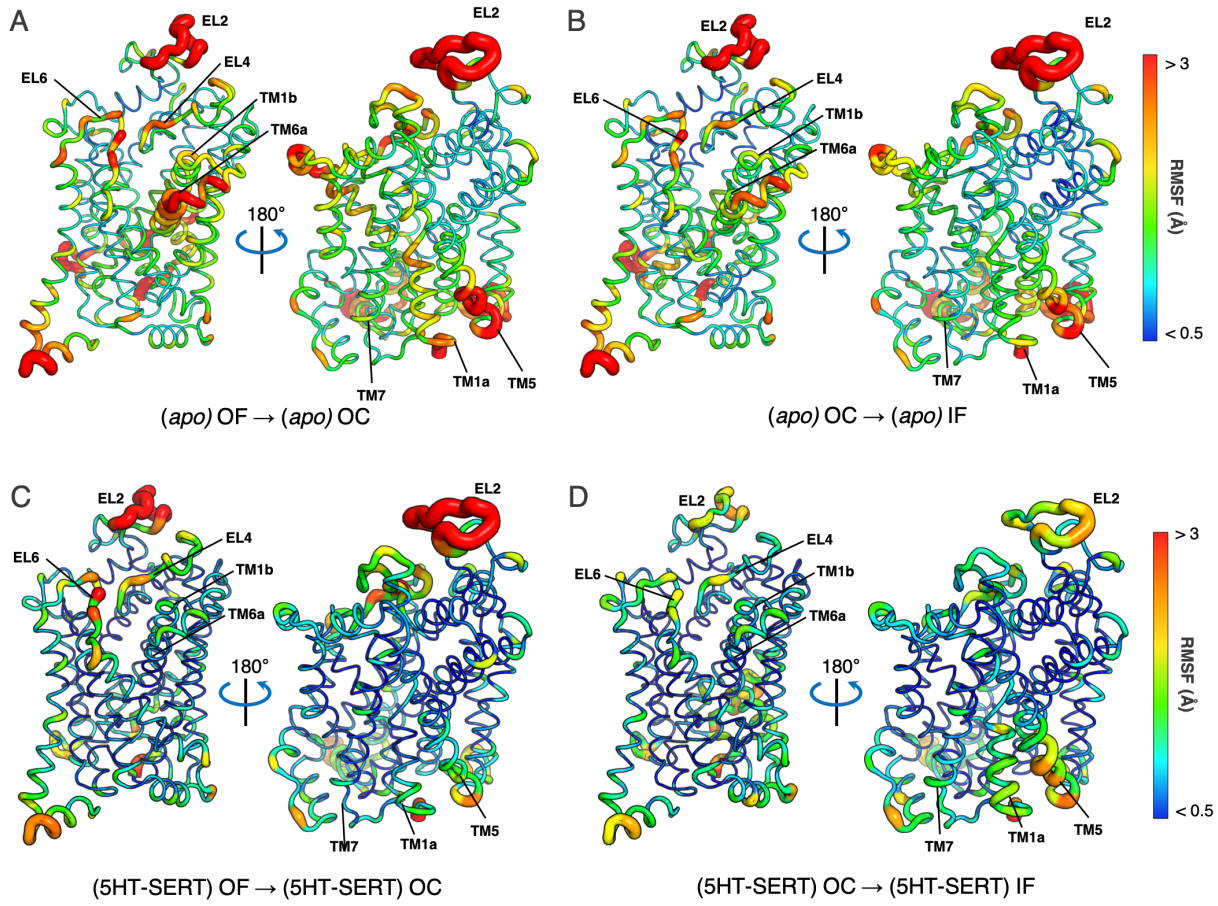

Figure 2: Molecular dynamics analysis of global fluctuations during conformational transitions. Root mean-squared fluctuations (RMSF) of *apo* (A,B) and 5HT transport (C,D) for OF to OC transition and OC to IF transition mapped to simulated SERT structure. Tube thickness corresponds to the RMSF values of each residue.

The calculated root mean squared fluctuation (RMSF) plots illustrate that in both *apo* and 5HT-SERT simulations, EL2 and EL4 are highly flexible during the OF to OC transitions. Alternatively, the loop regions are more stable during OC to IF in 5HT-SERT simulations compared to *apo* simulations (Figure 2). Hydrogen deuterium exchange (HDX) mass spectroscopy studies hint that EL2 and EL4 regions are destabilized and show increased deuterium exchange upon ion and substrate binding.[28,61,63,71] Furthermore, EL2 exhibits higher deuterium uptake kinetics in the OF state compared to the IF state in LeuT.[28] In 5HT-SERT simulations, EL4 shows less pronounced fluctuations during OC to IF transitions. The experimental results from HDX show EL4 regions are more stabilized during K^+ uptake which is hypothesized to stabilize SERT in an IF manner.[63,72] The increased deuterium uptake of TM1a in the presence of K^+ agrees with the large fluctuations we observed for transitions to the IF state. The comparison of calculated deuterium exchange fraction of *apo* and 5HT-SERT simulation data agree with previous HDX studies (Figure S4).[28]

Identification of a new sodium ion binding site in a buried cavity stabilizes the fold for substrate transport.

Monoamine transporters utilize an electrochemical gradient to transport substrates across the cellular membrane. 5HT-mediated transport involves the symport of 1 Na^+ and 1 Cl^- ion, in addition to 1 K^+ exported.[20,73] Upon the transition of 5HT from the allosteric to the orthosteric binding site, the Na^+ ion in the Na1 site shifts to a third metal coordination center, which we call the Na3 site to be consistent with prior nomenclature.[74,75] Here, Na^+ is coordinated by the carboxylates of Glu136 and Glu508, and the sulfur of Met135 through water molecules (Figure 3). A third metal ion site has not previously been described in SERT, but computational modeling, biochemical analysis, and electrophysiology recordings indicate that equivalent residues of the neuronal GlyT2 transporter also form a third Na^+ site.[75] We note that the presence of buried glutamates within hydrophobic transmembrane regions is highly unusual; in this case, Glu136 hydrogen bonds to exposed backbone N-H

groups to support the unwinding of TM6 near the central substrate binding site.

The simulation reveals that the presence of Na^+ in the Na3 site stabilizes TM6 unwinding and the proper orientations of residues in the orthosteric site. There are two pieces of experimental evidence for this *in silico* discovery. First, a structural alignment of SERT from the MD simulation with the crystal structure shows weak but discernible electron density, comparable to the density of surrounding side chains, near the modeled third Na^+ (Figure 3). Second, previous experiments have shown a reduction of serotonin transport when Glu136 is mutated, underscoring the role of this residue for appropriate conformational dynamics.[76]

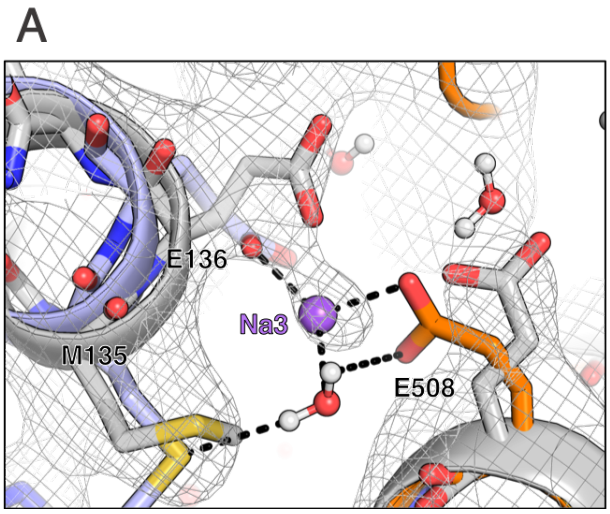

Figure 3: A third Na^+ ion binding site buried beneath the orthosteric pocket. MD snapshot (TM2 colored pale blue and TM10 orange) superimposed with the SERT crystal structure (PDB 5I73, grey), with electron density shown at 0.5 σ.

Simulations reveal a sequential order of substrate binding and transport in SERT.

An aspect of the current NSS transport model that remains unaddressed is the sequential order of substrate binding and transport events. Using transition path theory (TPT), the highest flux pathway for conformational change and 5HT import was determined and used

to predict an ordered sequence of binding events and structural changes. SERT undergoes complete transitions to the IF state in the simulations, with permeation towards the intracellular side upon binding of substrates in the order following Na^+, 5HT, and Cl^- ions (Figure 4). We describe each step of the import process in detail.

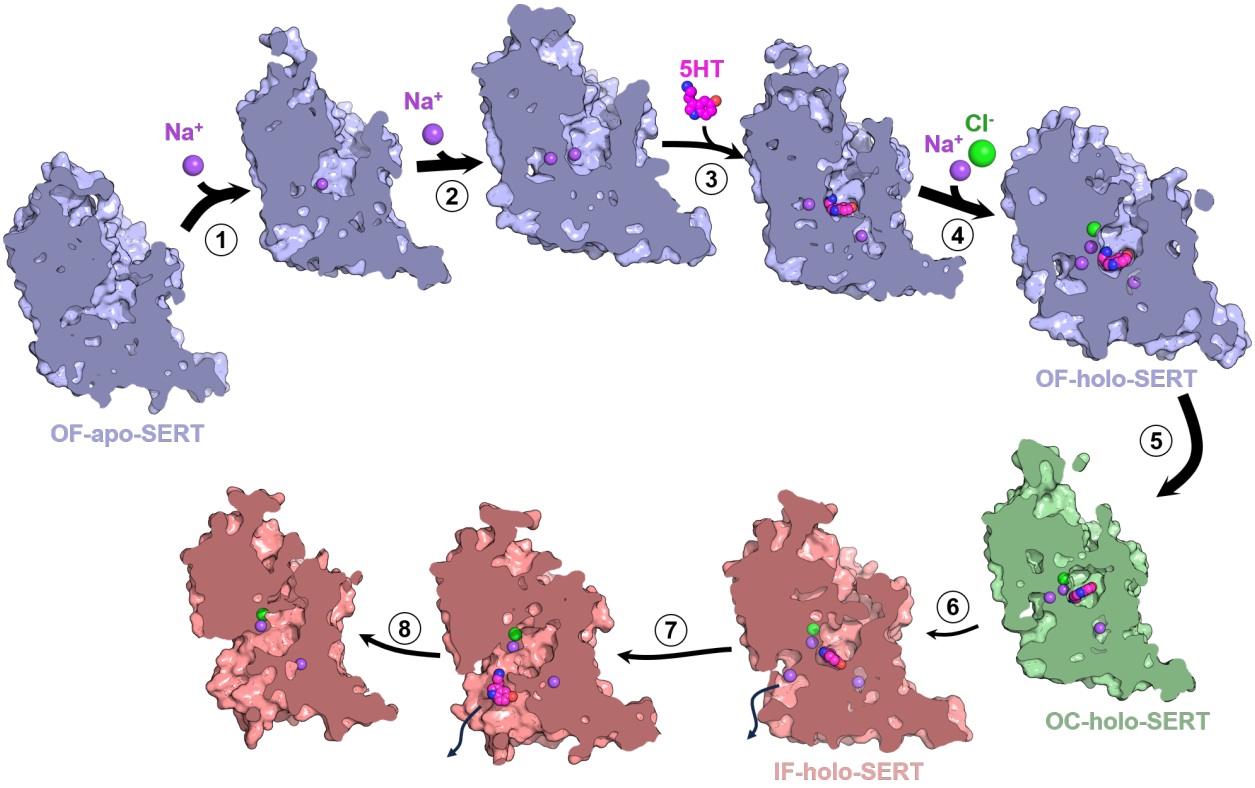

Figure 4: The major flux pathway of SERT conformational transitions and 5HT import determined from transition path theory. The transport process begins with the binding of 2 Na^+ ions to the Na1 and Na2 sites in the OF state (1, 2). Substrate diffusion to the orthosteric site shifts a Na^+ to the Na3 site (3). An additional Na^+ and Cl^- ion bind (4), facilitating closure of the extracellular gate to form the OC state (5). Isomerization to the IF state is associated with the release of Na^+ from the Na2 site and 5HT diffuses out (6-8). Arrow thickness represents relative flux between transitions.

The transport process begins with the binding of Na^+ to the high affinity Na1 site, followed by a second Na^+ binding the Na2 site. These two sites are well-described in the SERT crystal structure and the literature.[35,51,53,77] Na^+ bound at the Na1 site couples activity between the ion and substrate binding sites, whereas computational studies of related

transporters have indicated that Na^+ coordinated at the Na2 site dissociates during the transporter cycle to become the symported metal ion.[78] The importance of the Na2 site is underscored by its conservation in distantly related secondary transporters.[79] Na^+ ions entering the transporter interact with Asp328 and Asn112 at the extracellular surface, then rapidly diffuse into the allosteric site, a region where drugs bind to allosterically inhibit transport activity[51,80] (Figure S5A). Here, the Na^+ ions interact with Glu493 and Glu494, and a rotameric shift in Glu493 enables the ions to descend past the extracellular gate to their central binding sites (Figure S5A). Na1 is stabilized by Asn101, Ser336, and Asn368, while Na2 is coordinated by backbone carbonyls of Gly94, Val97, Leu434, and side chains of Asp437 and Ser438. Mutations of Asp437 and Ser438 have confirmed their role in coordination with Na^+ and alter ion dependency.[81] The binding of Na^+ ions to their respective sites neutralizes the polar cavity to allow protonated 5HT diffusion.

5HT is recognized by Tyr107, Ile108, Gln111, and Asp328 at the extracellular vestibule to initiate the binding in the OF state. Ile108 forms hydrophobic contacts with the indole ring of 5HT while other residues form polar interactions with the substrate that favors binding. 5HT then diffuses inside the translocation pore and binds to the allosteric site (Figure 5B). The substrate is stabilized by aromatic ring packing against Phe335 and Arg104, and a hydrogen bonding network with Asp328, Gln332, and Glu494 (Figure 5B). Previous mutations of residues in the allosteric site have been shown to alter inhibitor potency.[82] 5HT undergoes a 90° rotation by rapidly exchanging its polar interactions and shifts towards the orthosteric site. The switching of amine group interactions to Glu494 triggers the movement of 5HT from the allosteric site to the orthosteric site. 5HT rotates such that the conformation becomes perpendicular to the membrane which is further favored by polar and hydrophobic interactions by Asp328, Gln332, Leu502, and Ala331. The extracellular gating residues form a salt bridge interaction and enlarges the binding cavity such that substrate can escape to the primary binding site. In the orthosteric site, the protonated amine moiety of 5HT forms charged interactions with Asp98 of subsite A and aromatic interactions with Tyr95

and Phe341 in subsite A. This orthosteric binding site in the NSS family contains three well-studied subsites and has served as the basis of designing various tricyclic antidepressant molecules.[83] The biochemical studies show that the disruption of aromatic interactions with the substrate leads to a loss of function or decreased potency of antidepressants.[82,84] The binding of 5HT from the allosteric to the orthosteric binding site promotes Na^+ in the Na2 site to migrate to the third metal coordination center, the Na3 site.

5HT mediates the binding of an electrogenic Cl^- ion.

Cl^- and Na^+ permeate into the extracellular vestibule and bind at the Cl^- and vacated Na1 coordination sites, which lead to the formation of an occluded conformation. Na^+ is stabilized by Glu493 and Glu494 while Cl^- forms polar interactions with Arg104 and Tyr176. The additional interaction of Cl^- with the indole-NH of 5HT further stabilizes the ion in the exposed extracellular recognition site (Figure 5C). The indole ring of 5HT occupies subsite C of the primary binding site, which in turn favors the transition of the Cl^- ion to its binding site (Figure S6).

As Cl^- enters, it shifts the guanidinium group of Arg104, facilitating the diffusion of both the Cl^- and Na^+ ions into the central cavity (Figure S5C). The movement of Cl^- through the transporter is supported by a network of interactions with Arg104, Tyr176, and the indole-NH of 5HT (Figure 5C). A shift of the Arg104 side chain exposes Gln332 for making contacts with the Cl^- ion, facilitating its migration to the Cl^- binding site. The predicted Na1, Na2, and Cl^- sites in the simulations concur with their respective sites observed in crystal structures of SERT, LeuT, and DAT[35,51,53,77] (Figure S7).

The binding of ions to their respective sites leads to the closure of the extracellular gates to obtain the OC state where the translocation pore channel is closed at both ends. The decrease in pore channel radii results in shifting of the aromatic ring of 5HT from subsite C to subsite B within the orthosteric binding pocket. The amine moiety of the neurotransmitter remains bound to Asp98, Tyr95, and the C-terminal pole of TM1a within subsite A (Figure

5D). The simulated configuration of 5HT in subsite B agrees with the crystal structure of dopamine-bound DAT[77] (Figure S7F), and is further supported by several studies showing that interactions in subsite B are critical for inhibitor potency.[83–85] The indole-NH ring of 5HT interacts with Thr473 and other hydrophobic contacts by Ala169, Ala441, Gly442, and Leu443 residues stabilizing the substrate in subsite B. Previous experimental studies indicate that the mutations of these residues have been shown to decrease 5HT transport.[82,84]

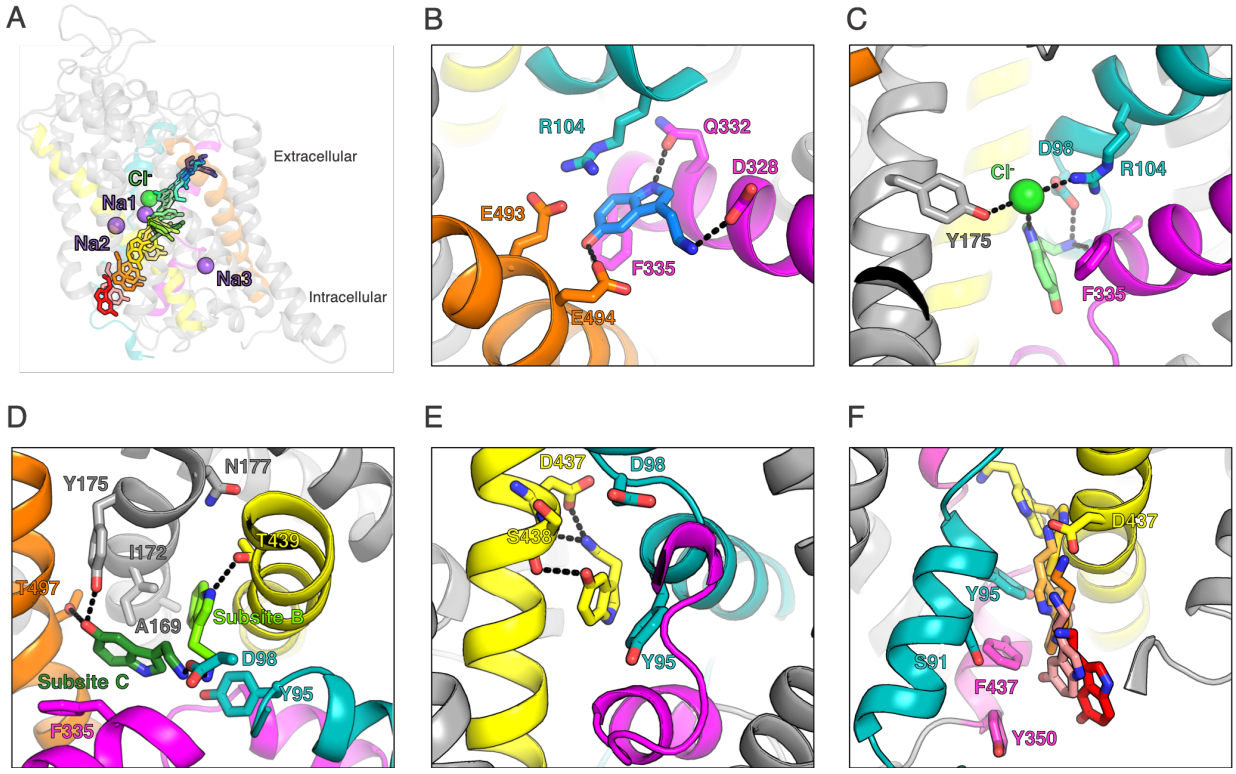

Figure 5: MD snapshots of the simulated mechanism for SERT-catalyzed 5HT import. (A) Overlaid MD snapshots of 5HT translocation, from when 5HT enters the extracellular vestibule (blue) to its cytosolic exit (red). The positions of ions in the OC state are shown as spheres. Transmembrane helices 1, 6, 8, and 10, are colored in teal, magenta, yellow, and orange, respectively. (B) 5HT enters the transporter by binding in the allosteric site. (C) Initial Cl- recognition is assisted by Asp98, Arg104, Tyr175, Phe335, and indole of 5HT. (D) The aromatic ring of 5HT transitions from subsite C to B. (E) Flipping of the phenol ring of Tyr95 initiates the permeation of 5HT towards the intracellular exit pathway. (F) 5HT translocation through the exit pathway.

Mechanism of 5HT translocation down the exit pathway.

The conformational free energy landscape suggests that structural isomerization to the IF state is limited by a large free energy barrier which is decreased in the presence of the substrate. The prolonged binding of 5HT in subsite B weakens Na^+ interactions in the Na2 site and results in its dissociation. Na^+ loses its interaction with the backbone carbonyl of Leu434 and enters the intracellular vestibule, thereby initiating structural transitions from the OC to IF state. The solvation of the intracellular cavity allows for the side chain rotation of Asp437, which coordinates Na^+ in the Na2 site, towards the exit pathway (Figure S8). The dissociated Na^+ interacts with Asp87 and Ser91 and diffuses into the intracellular space. At this juncture, the intracellular gating residues (Arg79 and Asp452) still hold its hydrogen bond interactions, and Na^+ can access the intracellular cavity without the breakage of ionic contacts. The coupling of 5HT import to the cytoplasmic release of Na^+ from the Na2 site explains the 1:1 sodium to neurotransmitter stoichiometry of the transport cycle.

The rotameric shift of Tyr95 results in permeation of 5HT to the exit pathway (Figure 5E). The flipping of the indole ring of 5HT displaces the ionic interactions with Asp98 resulting in the aromatic ring of 5HT to be trapped between Tyr95 and Val343. The 'downward' movement of 5HT weakens the intracellular salt bridge and results in the opening of the cytoplasmic cavity. 5HT shifts to the intracellular vestibule and occupies the Na2 site (Figure 5E). The amine group forms strong polar contacts with residues in the Na2 site, and the indole ring is lodged between Tyr95, Phe347, and Phe440. 5HT further diffuses down, however the amine group of 5HT still forms interactions with Tyr95, and the indole-NH forms additional interactions with Ser91. Finally, 5HT leaves the transporter and enters the intracellular space by interacting with Tyr350. Our results show that the rotation of Tyr95 propagates the opening of TM1a and mediates substrate transport to the cytoplasmic half. We also observed that the cytoplasmic base of TM5 shifts outwards by $\sim$4 Å to facilitate cytoplasmic opening of the exit pathway (Figure 5F), and it is well known that these regions play a crucial role in regulating SERT activity.[86]

Simulations identify key residues involved in serotonin transport.

SERT has been extensively studied by targeted mutagenesis, especially within the orthosteric binding site, confirming key interacting residues with substrate and drugs.[83,84] To validate aspects of the simulations, we instead focused mutagenesis to residues predicted to make early interactions with 5HT (Figure 6A). Changes in transport activity were assessed based on cellular uptake of a fluorescent 5HT analogue,[87] measured at a substrate concentration close to the transporter's K_M.

Alanine substitutions of Tyr107 and Gln111, which are predicted to participate in the early recognition of 5HT as it first diffuses into the extracellular vestibule, reduce substrate transport significantly, while mutations Ile108Ala and Asp328Ala in the allosteric site exhibit dramatic effects (Figure 6B). Both mutations are deleterious for transport activity as they mediate crucial interactions with the substrate in the initial recognition as well as in the allosteric site. (Figure 6B and C). Ile108 forms extensive hydrophobic contacts with the 5HT indole ring while Asp328 forms ionic contacts with the amine moiety of 5HT (Figure 6C). Leu502 is packed beneath aromatic residues in the allosteric and early recognition sites, and disruption of local structure by its substitution to alanine renders SERT inactive, although we cannot exclude broader effects on the protein fold (Figure 6D). We further tested alanine substitution of Val343, which is packed against Tyr95 at the base of the orthosteric site. Once Tyr95 undergoes a rotameric shift during the OC to IF transition, a void is created between Val343 and Tyr95 that is temporarily occupied by the substrate as it moves into the intracellular vestibule (Figure 6E). SERT Val343Ala has partly reduced activity, which is notable considering the close chemical similarity between alanine and valine side chains. Finally, Glu136 and Glu508 that coordinate Na^+ in the Na3 site were mutated to alanine to cause a complete loss of activity, demonstrating the importance of this region for the transport process.

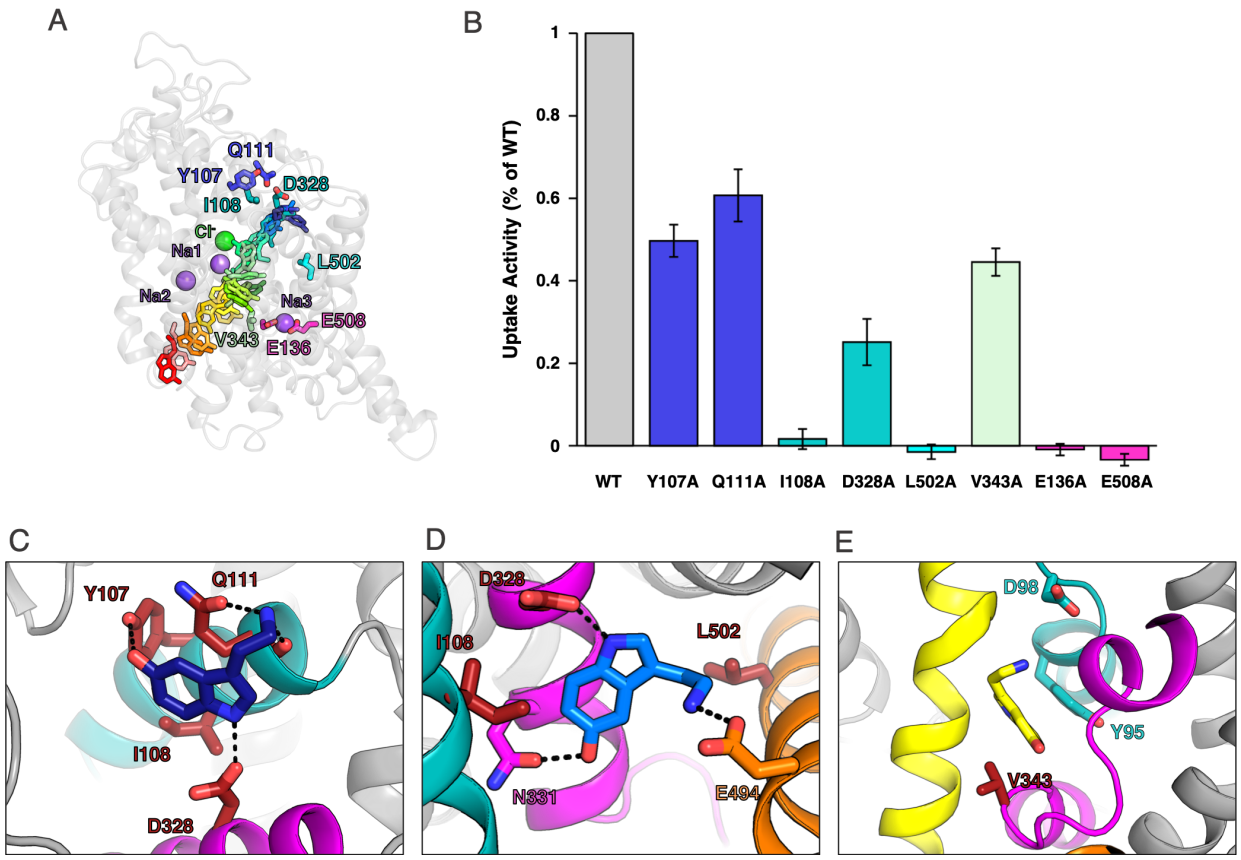

Figure 6: Alanine substitutions of residues involved in the simulated transport process cause decreased substrate uptake. (A) Overlaid MD snapshots showing the permeation of 5HT from its diffusion into the extracellular vestibule (dark blue), to binding at the orthosteric site (green), to cytosolic release (red). Mutated residues are similarly colored based on when in the import pathway they interact with 5HT. Glutamates coordinating Na^+ in the Na3 site are magenta. (B) SERT mutants were expressed in human Expi293F cells and uptake of fluorescent substrate APP+ was compared to wild type (WT) protein. Data are mean ± SD, n = 3. (C-E) MD snapshots of 5HT at the (C) extracellular vestibule, (D) allosteric site, and (E) released from the orthosteric site. Residues that were substituted with alanine colored as red sticks. Transmembrane helices 1, 6, 8, and 10, are colored in teal, magenta, yellow, and orange, respectively.

Conclusions

In this study, we present an atomistic view of the substrate import process in SERT as well as characterizing the thermodynamics of key states involved in substrate transport. By implementing an MSM-based adaptive sampling protocol to sample the conformational

landscape, we investigated global transitions from OF to IF for both 5HT-free and 5HT-transporting SERT. MSM-weighted conformational free energy landscapes show the OF and OC states are relatively stable, and transitions to and from OF and OC states are relatively low energy. Transitions from OC to IF are substantially higher, with energy barriers of $\sim$3 kcal/mol in 5HT-free SERT; however, the presence of 5HT in the transporter stabilizes the IF state and decreases the energy barrier to $\sim$1.5 kcal/mol. The dependence of the IF state on the presence of substrate has experimentally been observed for the bacterial LeuT transporter, where addition of extracellular substrate promotes dynamics at the intracellular gate.[67]

Our simulations reveal an ordered sequence of binding and transport events that agree with the 1:1 substrate:Na^+ stoichiometry as previously characterized for the NSS family. In doing so, we identified a third sodium ion binding site conserved among various NSS transporters that is critical for substrate transport. Release of Na^+ from the Na2 site decouples the interactions between TM1 and TM8 to allow for opening of TM1a for substrate release to the intracellular vestibule. From our simulations, we investigated the mechanism 5HT binding and translocation in SERT, which we further validated using mutagenesis experiments to confirm important interactions. Charged interactions at the allosteric site allow for 5HT to be recognized and enter the extracellular vestibule. The amine group of 5HT forms a stable cation-pi interaction with conserved Tyr95. This residue facilitates substrate release and must undergo a rotameric flip to allow 5HT to shift towards the intracellular exit pathway. Equivalent residues in DAT (Phe76) and NET (Phe72) may have analogous interactions and roles for substrate binding and transport.

Helical rearrangements observed in simulations closely match hydrogen-deuterium exchange experiments of LeuT.[28] Moreover, when compared to the recent cryo-EM structures,[57] we observed minimal helical fluctuations of TM1b, TM6a, and TM10, suggesting the role of the electrostatic interactions between Arg104 and Glu493 form a hydrogen bonding network that governs the opening and closing of the extracellular gate. Isomerization to

the inward-facing state is associated with an outward swinging motion of TM1a. We also note additional outward motions of TM7 and TM5 to facilitate opening of the intracellular vestibule and substrate release. We expect a similar mechanism of substrate induced conformational dynamics in related monoamine transporter DAT and NET.

Monoamine transporters SERT, DAT, and NET are critical molecular targets for the treatment of neurological disorders and drugs of abuse. These proteins share similar folds with high sequence similarity and only slight amino acid variations in the orthosteric binding sites. However, the molecular basis of how these transporters recognize their respective cognate substrates remains unclear. The work presented in this study provides an extensive perspective into the molecular recognition and translocation of 5HT.

Our simulations have explored the dynamics and transport of a monomeric unit of SERT; however, fluorescent microscopy has shown SERT to form functional oligomers in the membrane.[88,89] However, the exact interface of SERT oligomerization and the effects of coupled dynamics remains unclear. Further investigation is required into understanding how *in vivo* regulation affects the kinetics and conformational landscape of SERT.

Methods

Molecular dynamics (MD) simulations.

The OF SERT crystal structure (PDB: 5I73) was used as the starting model for MD simulation.[51] Thermostable mutations in the crystal structure Ala110, Ala291, and Ser439 were reverted to wild type Tyr110, Ile291, and Thr439, respectively. The protein was embedded in a phosphatidylcholine (POPC) bilayer with CHARMM-GUI[90] and solvated with TIP3P water molecules.[91] 150 mM NaCl was added to neutralize the system and mimic physiological conditions. Terminal chains were capped with acetyl and methyl amide groups. Overall, the final apo-SERT system consisted of ∼70,000 atoms in a period box volume of 77 X 77 X 113 Å^3. The MD system was built using the tleap module of AMBER14.[92] The MD system

was minimized for 20,000 steps using the conjugate gradient method, heated from 0 to 300 K at NVT, and equilibrated for 40 ns under NPT conditions. A Na^+ bound in the Na1 and Na2 site OF SERT structure, obtained from *apo*-SERT simulations, was used as the starting model to capture the mechanism of 5HT import. 100 mM serotonin (equivalent to 12 5HT molecules was randomly added to the simulation box and equilibrated under the same conditions described previously. All simulations were implemented using Amber14 package[92–95] employing Amber ff14SB[96] force field combined with GAFF force field at constant NPT conditions (300K, 1 atm) and periodic boundary conditions. Temperature and pressure were maintained with Berendsen thermostat and barostat, respectively.[97] Electrostatic interactions were treated with the Partial Mesh Ewald method,[98] and hydrogen bonds were constrained using SHAKE algorithm.[99] Nonbonded distance cutoff was set at 10 Å, and an integration timestep of 2 fs was used for all simulations. Snapshots were saved every 100 ps during production simulations.

Adaptive sampling.

Obtaining sufficient sampling is a reoccurring challenge in simulating complex biological processes. To overcome this issue, we adopted a Markov state model (MSM)-based adaptive sampling methodology to efficiently explore the conformational landscape.[64,100,101] In each round of adaptive sampling, multiple short MD simulations are conducted in parallel. The simulation data is clustered using the K-means algorithm[102] based on a designated metric and starting structures are chosen from the least populated states to seed the subsequent rounds of simulation. This sampling bias is eliminated during the construction of the MSM by estimating the reverse transition probability matrix for transition between all conformational states. Extracellular and intracellular gating residues as adaptive sampling metrics for the conformational sampling of the states and z-position of substrates to capture the import process. A total of $\sim$130 μs of *apo*- and $\sim$170 μs 5HT transport simulation data was obtained. The entire MD dataset was used for MSM construction and analysis.

MSM construction.

CPPTRAJ[103] module in AmberTools and MDTraj[104] was used for post processing the trajectory data. Markov state models (MSMs) were constructed using pyEMMA 2.5.6 Python package.[105] MSMs were constructed for both *apo*- and 5HT transport datasets. 13 residue-residue pair distances surrounding the channel pore radius were chosen as featurization metrics for clustering of *apo*-SERT (Figure S9). The z-components of 5HT, Cl^-, and the symported Na^+ ion were added along with the 13 distances for the 5HT transport process. The optimum number of clusters were obtained by using the VAMP score hyperparameter optimization tool implimented in pyEMMA. 700 clusters were used for both *apo*- and 5HT transport datasets to construct MSMs (Figure S10A). The lag time of 8 ns was determined for MSM construction from implied timescale plots (Figure S10B). Chapman-Kolmogorov test, which validates the Markovian behavior of the MSM,[106] was performed on 5 macrostates implemented in pyEMMA (Figure S11 and S12).

Trajectory analysis.

MSM-weighted simulation data was plotted on the coordinates of the gating distances, specifically the closest heavy atom between Arg104 and Glu493 for the extracellular gate, and closest heavy atom distance between residues 77-81 of the N-terminus tail and residues 450-455 of TM8 for the intracellular gate. The predicted fraction deuteration was calculated according to Adhikary et al.[28] on 700 OF and IF structures randomly extracted from the *apo*-SERT and 5HT-SERT MSM. The top flux pathways for conformational changes and 5HT transport were determined using transition path theory (TPT) analysis implemented in pyEMMA . TPT examines the transition probabilities and estimates transitions pathways connecting the source and sink states and the flux associated with the pathway.[107] MSM states were further clustered into macrostates and visualized with Visual Molecular Dynamics (VMD)[108] and PyMOL (Shrodinger, LLC). The 5HT-residue interactions were obtained from python scripts implemented from the GetContacts package (https://getcontacts.github.io/). To cal-

culate the RMSF between transitions, 1000 structures of each OF, OC, and IF states were randomly extracted from the MSM and measured with respect to the cryo-EM structure of the prior conformational state (i.e. OF-OC: 1000 OC structures with respect to OF cryo-EM structure). In-house scripts and matplotlib Python library were used to generate plots. Channel pore radius was calculated using the HOLE program.[109]

Plasmid Construction

Human SERT was PCR amplified from pcDNA3-*h*SERT (Addgene 15483)[110] to introduce a consensus Kozak sequence and ligated into the Kpn1-Xho1 sites of pCEP4 (Invitrogen). Alanine substitutions were introduced by overlap extension PCR, and all plasmid sequences were verified.

Transport Assay

Expi293F cells (ThermoFisher) were cultured in Expi293F expression medium (ThermoFisher) at 37°C, 8% CO_2, 125 rpm, and transfected with 500 ng plasmid per ml at a density of 2 x 10^6 cells/ml using Expifectamine (ThermoFisher). 24-28 hr post-transfection, cells were washed with PBS-BSA (Dulbecco's phosphate-buffered saline supplemented with 0.2% bovine serum albumin), incubated with 0.5 μM fluorescent substrate analogue APP+ (Aobious) in PBS-BSA for 2 min at room temperature, washed twice with ice cold PBS-BSA, and analyzed on a BD LSRII cytometer. Fluorescence corresponding to non-specific uptake by mock transfected cells was subtracted, and activity of mutants was assessed relative to the wild type construct.

Author Information

Corresponding Author

Email: diwakar@illinois.edu, procko@illinois.edu

Funding sources

This work was funded by NSF MCB 18-45606 to DS. EP is supported by R21 MH113155 from NIMH.

Notes

The authors declare no competing financial interest.

Acknowledgement

The authors thank the Blue Waters sustained-petascale computing project, which is supported by the National Science Foundation (awards OCI-0725070 and ACI-1238993) and the state of Illinois. Blue Waters is a joint effort of the University of Illinois at Urbana-Champaign and its National Center for Supercomputing Applications.

Abbreviations

SERT, serotonin transporter; 5HT, 5-hydroxytryptamine; DAT, dopamine transporter; NET, norepinephrine transporter; NSS, neurotransmitter:sodium symporter; TM, transmembrane; LeuT, leucine transporter; OF, outward-facing; OC, occluded; IF, inward-facing; *d*DAT, *Drosophila* dopamine transporter; *h*SERT, human serotonin transporter; EL, extracellular loop; HDX, hydrogen-deuterium exchange; MSM, Markov state model.

References

(1) Holmes, A.; Murphy, D. L.; Crawley, J. N. Abnormal behavioral phenotypes of serotonin transporter knockout mice: parallels with human anxiety and depression. *Biological Psychiatry* **2003**, *54*, 953–959.

(2) Jacobs, B. L.; Azmitia, E. C. Structure and function of the brain serotonin system. *Physiological Reviews* **1992**, *72*, 165–229.

(3) Murphy, D. L.; Uhl, G. R.; Holmes, A.; Ren-Patterson, R.; Hall, F. S.; Sora, I.; Detera-Wadleigh, S.; Lesch, K.-P. Experimental gene interaction studies with SERT mutant mice as models for human polygenic and epistatic traits and disorders. *Genes, Brain and Behavior* **2003**, *2*, 350–364.

(4) Zhuang, X.; Gross, C.; Santarelli, L.; Compan, V.; Trillat, A.-C.; Hen, R. Altered Emotional States in Knockout Mice Lacking 5-HT1A or 5-HT1B Receptors. *Neuropsychopharmacology* **1999**, *21*, 52.

(5) Devlin, B.; Cook, E. H.; Coon, H.; Dawson, G.; Grigorenko, E. L.; McMahon, W.; Minshew, N.; Pauls, D.; Smith, M.; Spence, M. A.; Rodier, P. M.; Stodgell, C.; Schellenberg, G. D. Autism and the serotonin transporter: the long and short of it. *Molecular Psychiatry* **2005**, *10*, 1110.

(6) Jr, E. C.; Courchesne, R.; Lord, C.; Cox, N. J.; Yan, S.; Lincoln, A.; Haas, R.; Courchesne, E.; Leventhal, B. L. Evidence of linkage between the serotonin transporter and autistic disorder. *Molecular Psychiatry* **1997**, *2*, 247.

(7) Kilpatrick, D. G.; Koenen, K. C.; Ruggiero, K. J.; Acierno, R.; Galea, S.; Resnick, H. S.; Roitzsch, J.; Boyle, J.; Gelernter, J. The Serotonin Transporter Genotype and Social Support and Moderation of Posttraumatic Stress Disorder and Depression in Hurricane-Exposed Adults. *American Journal of Psychiatry* **2007**, *164*, 1693–1699.

(8) Kunugi, H.; Hattori, M.; Kato, T.; Tatsumi, M.; Sakai, T.; Sasaki, T.; Hirose, T.; Nanko, S. Serotonin transporter gene polymorphisms: ethnic difference and possible association with bipolar affective disorder. *Molecular Psychiatry* **1997**, *2*, 457.

(9) Lee, H.-J. et al. Influence of the serotonin transporter promoter gene polymorphism on susceptibility to posttraumatic stress disorder. *Depression and Anxiety* **2005**, *21*, 135–139.

(10) Ni, W.; Watts, S. W. 5-Hydroxytryptamine in the Cardiovascular System: Focus on the Serotonin Transporter (sert). *Clinical and Experimental Pharmacology and Physiology* **2006**, *33*, 575–583.

(11) Jedlitschky, G.; Greinacher, A.; Kroemer, H. K. Transporters in human platelets: physiologic function and impact for pharmacotherapy. *Blood* **2012**, *119*, 3394–3402.

(12) Gether, U.; Andersen, P. H.; Larsson, O. M.; Schousboe, A. Neurotransmitter transporters: molecular function of important drug targets. *Trends in Pharmacological Sciences* **2006**, *27*, 375–383.

(13) Rudnick, G.; Wall, S. C. The molecular mechanism of "ecstasy" [3,4-methylenedioxymethamphetamine (MDMA)]: serotonin transporters are targets for MDMA-induced serotonin release. *Proceedings of the National Academy of Sciences* **1992**, *89*, 1817–1821.

(14) Blakely, R. D.; DeFelice, L. J.; Galli, A. Biogenic Amine Neurotransmitter Transporters: Just When You Thought You Knew Them. *Physiology* **2005**, *20*, 225–231.

(15) Gouaux Eric, The molecular logic of sodium-coupled neurotransmitter transporters. *Philosophical Transactions of the Royal Society B: Biological Sciences* **2009**, *364*, 149–154.

(16) Henry, L. K. et al. A Conserved Asparagine Residue in Transmembrane Segment 1 (TM1) of Serotonin Transporter Dictates Chloride-coupled Neurotransmitter Transport. *Journal of Biological Chemistry* **2011**, *286*, 30823–30836.

(17) Kanner, B. I. Sodium-coupled neurotransmitter transport: structure, function and regulation. *Journal of Experimental Biology* **1994**, *196*, 237–249.

(18) Krishnamurthy, H.; Piscitelli, C. L.; Gouaux, E. Unlocking the molecular secrets of sodium-coupled transporters. *Nature* **2009**, *459*, 347–355.

(19) Nelson, P. J.; Rudnick, G. The role of chloride ion in platelet serotonin transport. *Journal of Biological Chemistry* **1982**, *257*, 6151–6155.

(20) Rudnick, G.; Nelson, P. J. Platelet 5-hydroxytryptamine transport, an electroneutral mechanism coupled to potassium. *Biochemistry* **1978**, *17*, 4739–4742.

(21) Jayanthi, L. D.; Ramamoorthy, S. Regulation of monoamine transporters: Influence of psychostimulants and therapeutic antidepressants. *The AAPS Journal* **2005**, *7*, E728–E738.

(22) Lin, F.; Lester, H. A.; Mager, S. Single-channel currents produced by the serotonin transporter and analysis of a mutation affecting ion permeation. *Biophysical Journal* **1996**, *71*, 3126–3135.

(23) Mager, S.; Min, C.; Henry, D. J.; Chavkintt, C.; Hoffman, B. J.; Davidson, N.; Lester, H. A. Conducting states of a mammalian serotonin transporter. *Neuron* **1994**, *12*, 845–859.

(24) Ruchala, I.; Cabra, V.; Solis, E.; Glennon, R. A.; De Felice, L. J.; Eltit, J. M. Electrical coupling between the human serotonin transporter and voltage-gated Ca2+ channels. *Cell Calcium* **2014**, *56*, 25–33.

(25) Schmid, J. A.; Just, H.; Sitte, H. H. Impact of oligomerization on the function of the human serotonin transporter. *Biochemical Society transactions* **2001**, *29*, 732–736.

(26) Forrest, L. R. Structural Symmetry in Membrane Proteins. *Annual Review of Biophysics* **2015**, *44*, 311–337.

(27) Yamashita, A.; Singh, S. K.; Kawate, T.; Jin, Y.; Gouaux, E. Crystal structure of a bacterial homologue of Na + /Cl- -dependent neurotransmitter transporters. *Nature* **2005**, *437*, 215.

(28) Adhikary, S.; Deredge, D. J.; Nagarajan, A.; Forrest, L. R.; Wintrode, P. L.; Singh, S. K. Conformational dynamics of a neurotransmitter:sodium symporter in a lipid bilayer. *Proceedings of the National Academy of Sciences* **2017**, *114*, E1786–E1795.

(29) Gur, M.; Zomot, E.; Cheng, M. H.; Bahar, I. Energy landscape of LeuT from molecular simulations. *The Journal of Chemical Physics* **2015**, *143*, 243134.

(30) Shi, L.; Quick, M.; Zhao, Y.; Weinstein, H.; Javitch, J. A. The Mechanism of a Neurotransmitter:Sodium Symporter—Inward Release of Na+ and Substrate Is Triggered by Substrate in a Second Binding Site. *Molecular Cell* **2008**, *30*, 667–677.

(31) Singh, S. K.; Pal, A. In *Methods in Enzymology*; Shukla, A. K., Ed.; Membrane Proteins—Engineering, Purification and Crystallization; Academic Press, 2015; Vol. 557; pp 167–198.

(32) Terry, D. S.; Kolster, R. A.; Quick, M.; LeVine, M. V.; Khelashvili, G.; Zhou, Z.; Weinstein, H.; Javitch, J. A.; Blanchard, S. C. A partially-open inward-facing intermediate conformation of LeuT is associated with Na + release and substrate transport. *Nature Communications* **2018**, *9*, 230.

(33) Forrest, L. R.; Zhang, Y.-W.; Jacobs, M. T.; Gesmonde, J.; Xie, L.; Honig, B. H.; Rudnick, G. Mechanism for alternating access in neurotransmitter transporters. *Proceedings of the National Academy of Sciences* **2008**, *105*, 10338–10343.

(34) Jardetzky, O. Simple Allosteric Model for Membrane Pumps. *Nature* **1966**, *211*, 969.

(35) Krishnamurthy, H.; Gouaux, E. X-ray structures of LeuT in substrate-free outward-open and apo inward-open states. *Nature* **2012**, *481*, 469–474.

(36) Mitchell, P. A General Theory of Membrane Transport From Studies of Bacteria. *Nature* **1957**, *180*, 134–136.

(37) Claxton, D. P.; Quick, M.; Shi, L.; de Carvalho, F. D.; Weinstein, H.; Javitch, J. A.; Mchaourab, H. S. Ion/substrate-dependent conformational dynamics of a bacterial homolog of neurotransmitter:sodium symporters. *Nature Structural & Molecular Biology* **2010**, *17*, 822–829.

(38) Kazmier, K.; Sharma, S.; Islam, S. M.; Roux, B.; Mchaourab, H. S. Conformational cycle and ion-coupling mechanism of the Na+/hydantoin transporter Mhp1. *Proceedings of the National Academy of Sciences* **2014**, *111*, 14752–14757.

(39) Kazmier, K.; Sharma, S.; Quick, M.; Islam, S. M.; Roux, B.; Weinstein, H.; Javitch, J. A.; Mchaourab, H. S. Conformational dynamics of ligand-dependent alternating access in LeuT. *Nature structural & molecular biology* **2014**, *21*, 472–479.

(40) Focke, P. J.; Wang, X.; Larsson, H. P. Neurotransmitter Transporters: Structure Meets Function. *Structure* **2013**, *21*, 694–705.

(41) Shaikh, S. A.; Tajkhorshid, E. Modeling and dynamics of the inward-facing state of a Na+/Cl- dependent neurotransmitter transporter homologue. *PLoS computational biology* **2010**, *6*, e1000905.

(42) Zhao, Y.; Terry, D.; Shi, L.; Weinstein, H.; Blanchard, S. C.; Javitch, J. A. Single-molecule dynamics of gating in a neurotransmitter transporter homologue. *Nature* **2010**, *465*, 188–193.

(43) Cheng, M.; Bahar, I. Coupled Global and Local Changes Direct Substrate Translo-

cation by Neurotransmitter-Sodium Symporter Ortholog LeuT. *Biophysical Journal* **2013**, *105*, 630–639.

(44) Cheng, M. H.; Bahar, I. Complete Mapping of Substrate Translocation Highlights the Role of LeuT N-terminal Segment in Regulating Transport Cycle. *PLoS Computational Biology* **2014**, *10*.

(45) Andersen, J.; Stuhr-Hansen, N.; Zachariassen, L.; Toubro, S.; Hansen, S. M. R.; Eildal, J. N. N.; Bond, A. D.; Bøgesø, K. P.; Bang-Andersen, B.; Kristensen, A. S.; Strømgaard, K. Molecular determinants for selective recognition of antidepressants in the human serotonin and norepinephrine transporters. *Proceedings of the National Academy of Sciences* **2011**, *108*, 12137–12142.

(46) Mortensen, O. V.; Kortagere, S. Designing modulators of monoamine transporters using virtual screening techniques. *Frontiers in Pharmacology* **2015**, *6*.

(47) Schlessinger, A.; Geier, E.; Fan, H.; Irwin, J. J.; Shoichet, B. K.; Giacomini, K. M.; Sali, A. Structure-based discovery of prescription drugs that interact with the norepinephrine transporter, NET. *Proceedings of the National Academy of Sciences* **2011**, *108*, 15810–15815.

(48) Cheng, M.; Bahar, I. Molecular Mechanism of Dopamine Transport by Human Dopamine Transporter. *Structure* **2015**, *23*, 2171–2181.

(49) Cheng, M. H.; Kaya, C.; Bahar, I. Quantitative Assessment of the Energetics of Dopamine Translocation by Human Dopamine Transporter. *The Journal of Physical Chemistry B* **2018**, *122*, 5336–5346.

(50) Razavi, A. M.; Khelashvili, G.; Weinstein, H. A Markov State-based Quantitative Kinetic Model of Sodium Release from the Dopamine Transporter. *Scientific Reports* **2017**, *7*, 40076.

(51) Coleman, J. A.; Green, E. M.; Gouaux, E. X-ray structures and mechanism of the human serotonin transporter. *Nature* **2016**, *532*, 334–339.

(52) Gabrielsen, M.; Ravna, A. W.; Kristiansen, K.; Sylte, I. Substrate binding and translocation of the serotonin transporter studied by docking and molecular dynamics simulations. *Journal of Molecular Modeling* **2012**, *18*, 1073–1085.

(53) Penmatsa, A.; Wang, K. H.; Gouaux, E. X-ray structure of dopamine transporter elucidates antidepressant mechanism. *Nature* **2013**, *503*, 85–90.

(54) Xue, W.; Yang, F.; Wang, P.; Zheng, G.; Chen, Y.; Yao, X.; Zhu, F. What Contributes to Serotonin–Norepinephrine Reuptake Inhibitors' Dual-Targeting Mechanism? The Key Role of Transmembrane Domain 6 in Human Serotonin and Norepinephrine Transporters Revealed by Molecular Dynamics Simulation. *ACS Chemical Neuroscience* **2018**, *9*, 1128–1140.

(55) Wang, H.; Goehring, A.; Wang, K. H.; Penmatsa, A.; Ressler, R.; Gouaux, E. Structural basis for action by diverse antidepressants on biogenic amine transporters. *Nature* **2013**, *503*, 141–145.

(56) Coleman, J. A.; Gouaux, E. Structural basis for recognition of diverse antidepressants by the human serotonin transporter. *Nature Structural & Molecular Biology* **2018**, *25*, 170.

(57) Coleman, J. A.; Yang, D.; Zhao, Z.; Wen, P.-C.; Yoshioka, C.; Tajkhorshid, E.; Gouaux, E. Serotonin transporter–ibogaine complexes illuminate mechanisms of inhibition and transport. *Nature* **2019**, *569*, 141–145.

(58) Malinauskaite, L.; Quick, M.; Reinhard, L.; Lyons, J. A.; Yano, H.; Javitch, J. A.; Nissen, P. A mechanism for intracellular release of Na^+ by neurotransmitter/sodium symporters. *Nature Structural & Molecular Biology* **2014**, *21*, 1006–1012.

(59) Khelashvili, G.; Stanley, N.; Sahai, M. A.; Medina, J.; LeVine, M. V.; Shi, L.; De Fabritiis, G.; Weinstein, H. Spontaneous Inward Opening of the Dopamine Transporter Is Triggered by PIP2-Regulated Dynamics of the N-Terminus. *ACS Chemical Neuroscience* **2015**, *6*, 1825–1837.

(60) Kniazeff, J.; Shi, L.; Loland, C. J.; Javitch, J. A.; Weinstein, H.; Gether, U. An Intracellular Interaction Network Regulates Conformational Transitions in the Dopamine Transporter. *The Journal of Biological Chemistry* **2008**, *283*, 17691–17701.

(61) Möller, I. R.; Slivacka, M.; Nielsen, A. K.; Rasmussen, S. G. F.; Gether, U.; Loland, C. J.; Rand, K. D. Conformational dynamics of the human serotonin transporter during substrate and drug binding. *Nature Communications* **2019**, *10*, 1687.

(62) Nielsen, A. K.; Möller, I. R.; Wang, Y.; Rasmussen, S. G. F.; Lindorff-Larsen, K.; Rand, K. D.; Loland, C. J. Substrate-induced conformational dynamics of the dopamine transporter. *Nature Communications* **2019**, *10*, 2714.

(63) Merkle, P. S.; Gotfryd, K.; Cuendet, M. A.; Leth-Espensen, K. Z.; Gether, U.; Loland, C. J.; Rand, K. D. Substrate-modulated unwinding of transmembrane helices in the NSS transporter LeuT. *Science Advances* **2018**, *4*, eaar6179.

(64) Selvam, B.; Mittal, S.; Shukla, D. Free Energy Landscape of the Complete Transport Cycle in a Key Bacterial Transporter. *ACS Central Science* **2018**, *4*, 1146–1154.

(65) Husic, B. E.; Pande, V. S. Markov State Models: From an Art to a Science. *Journal of the American Chemical Society* **2018**, *140*, 2386–2396.

(66) Shukla, D.; Hernández, C. X.; Weber, J. K.; Pande, V. S. Markov State Models Provide Insights into Dynamic Modulation of Protein Function. *Accounts of Chemical Research* **2015**, *48*, 414–422.

(67) Zhao, Y.; Terry, D. S.; Shi, L.; Quick, M.; Weinstein, H.; Blanchard, S. C.; Javitch, J. A. Substrate-modulated gating dynamics in a Na^+-coupled neurotransmitter transporter homologue. *Nature* **2011**, *474*, 109–113.

(68) Sun, P.; Li, J.; Zhang, X.; Guan, Z.; Xiao, Q.; Zhao, C.; Song, M.; Zhou, Y.; Mou, L.; Ke, M.; Guo, L.; Geng, J.; Deng, D. Crystal structure of the bacterial acetate transporter SatP reveals that it forms a hexameric channel. *Journal of Biological Chemistry* **2018**, jbc.RA118.003876.

(69) Campbell, N. G. et al. Structural, functional, and behavioral insights of dopamine dysfunction revealed by a deletion in SLC6A3. *Proceedings of the National Academy of Sciences of the United States of America* **2019**, *116*, 3853–3862.

(70) Cao, Y. et al. Crystal structure of a potassium ion transporter, TrkH. *Nature* **2011**, *471*, 336–340.

(71) Machtens, J.-P.; Kortzak, D.; Lansche, C.; Leinenweber, A.; Kilian, P.; Begemann, B.; Zachariae, U.; Ewers, D.; de Groot, B.; Briones, R.; Fahlke, C. Mechanisms of Anion Conduction by Coupled Glutamate Transporters. *Cell* **2015**, *160*, 542–553.

(72) Billesbølle, C. B.; Mortensen, J. S.; Sohail, A.; Schmidt, S. G.; Shi, L.; Sitte, H. H.; Gether, U.; Loland, C. J. Transition metal ion FRET uncovers K+ regulation of a neurotransmitter/sodium symporter. *Nature communications* **2016**, *7*, 12755.

(73) Nelson, P. J.; Rudnick, G. Coupling between platelet 5-hydroxytryptamine and potassium transport. *J Biol Chem* **1979**, *254*, 10084–10089.

(74) Benito-Muñoz, C.; Perona, A.; Abia, D.; Dos Santos, H. G.; Núñez, E.; Aragón, C.; López-Corcuera, B. Modification of a Putative Third Sodium Site in the Glycine Transporter GlyT2 Influences the Chloride Dependence of Substrate Transport. *Frontiers in Molecular Neuroscience* **2018**, *11*, 347.

(75) Subramanian, N.; Scopelitti, A. J.; Carland, J. E.; Ryan, R. M.; O'Mara, M. L.; Vandenberg, R. J. Identification of a 3rd Na+ Binding Site of the Glycine Transporter, GlyT2. *PLOS ONE* **2016**, *11*, e0157583.

(76) Korkhov, V. M.; Holy, M.; Freissmuth, M.; Sitte, H. H. The Conserved Glutamate (Glu136) in Transmembrane Domain 2 of the Serotonin Transporter Is Required for the Conformational Switch in the Transport Cycle. *Journal of Biological Chemistry* **2006**, *281*, 13439–13448.

(77) Wang, K. H.; Penmatsa, A.; Gouaux, E. Neurotransmitter and psychostimulant recognition by the dopamine transporter. *Nature* **2015**, *521*, 322–327.

(78) Stolzenberg, S.; Li, Z.; Quick, M.; Malinauskaite, L.; Nissen, P.; Weinstein, H.; Javitch, J. A.; Shi, L. The role of transmembrane segment 5 (TM5) in Na2 release and the conformational transition of neurotransmitter:sodium symporters toward the inward-open state. *The Journal of Biological Chemistry* **2017**, *292*, 7372–7384.

(79) Khafizov, K.; Perez, C.; Koshy, C.; Quick, M.; Fendler, K.; Ziegler, C.; Forrest, L. R. Investigation of the sodium-binding sites in the sodium-coupled betaine transporter BetP. *Proceedings of the National Academy of Sciences* **2012**, *109*, E3035–E3044.

(80) Chen, F.; Larsen, M. B.; Neubauer, H. A.; Sánchez, C.; Plenge, P.; Wiborg, O. Characterization of an allosteric citalopram-binding site at the serotonin transporter. *Journal of Neurochemistry* **2005**, *92*, 21–28.

(81) Felts, B.; Pramod, A. B.; Sandtner, W.; Burbach, N.; Bulling, S.; Sitte, H. H.; Henry, L. K. The Two Na+ Sites in the Human Serotonin Transporter Play Distinct Roles in the Ion Coupling and Electrogenicity of Transport. `http://www.jbc.org`.

(82) Andersen, J.; Stuhr-Hansen, N.; Zachariassen, L. G.; Koldsø, H.; Schiøtt, B.; Strømgaard, K.; Kristensen, A. S. Molecular Basis for Selective Serotonin Reuptake

Inhibition by the Antidepressant Agent Fluoxetine (Prozac). *Molecular Pharmacology* **2014**, *85*, 703–714.

(83) Sørensen, L.; Andersen, J.; Thomsen, M.; Hansen, S. M. R.; Zhao, X.; Sandelin, A.; Strømgaard, K.; Kristensen, A. S. Interaction of antidepressants with the serotonin and norepinephrine transporters: mutational studies of the S1 substrate binding pocket. *The Journal of Biological Chemistry* **2012**, *287*, 43694–43707.

(84) Andersen, J.; Olsen, L.; Hansen, K. B.; Taboureau, O.; Jørgensen, F. S.; Jørgensen, A. M.; Bang-Andersen, B.; Egebjerg, J.; Strømgaard, K.; Kristensen, A. S. Mutational mapping and modeling of the binding site for (S)-citalopram in the human serotonin transporter. *The Journal of Biological Chemistry* **2010**, *285*, 2051–2063.

(85) Koldsø, H.; Severinsen, K.; Tran, T. T.; Celik, L.; Jensen, H. H.; Wiborg, O.; Schiøtt, B.; Sinning, S. The two enantiomers of citalopram bind to the human serotonin transporter in reversed orientations. *Journal of the American Chemical Society* **2010**, *132*, 1311–1322.

(86) Sørensen, L.; Strømgaard, K.; Kristensen, A. S. Characterization of intracellular regions in the human serotonin transporter for phosphorylation sites. *ACS chemical biology* **2014**, *9*, 935–944.

(87) Solis, E.; Zdravkovic, I.; Tomlinson, I. D.; Noskov, S. Y.; Rosenthal, S. J.; De Felice, L. J. 4-(4-(dimethylamino) phenyl)-1-methylpyridinium (APP+) is a fluorescent substrate for the human serotonin transporter. *Journal of Biological Chemistry* **2012**, *287*, 8852–8863.

(88) Anderluh, A.; Klotzsch, E.; Reismann, A. W. A. F.; Brameshuber, M.; Kudlacek, O.; Newman, A. H.; Sitte, H. H.; Schütz, G. J. Single molecule analysis reveals coexistence of stable serotonin transporter monomers and oligomers in the live cell plasma membrane. *The Journal of Biological Chemistry* **2014**, *289*, 4387–4394.

(89) Anderluh, A.; Hofmaier, T.; Klotzsch, E.; Kudlacek, O.; Stockner, T.; Sitte, H. H.; Schütz, G. J. Direct PIP_2 binding mediates stable oligomer formation of the serotonin transporter. *Nature Communications* **2017**, *8*, 14089.

(90) Jo, S.; Kim, T.; Iyer, V. G.; Im, W. CHARMM-GUI: a web-based graphical user interface for CHARMM. *Journal of computational chemistry* **2008**, *29*, 1859–1865.

(91) Jorgensen, W. L.; Chandrasekhar, J.; Madura, J. D.; Impey, R. W.; Klein, M. L. Comparison of simple potential functions for simulating liquid water. *The Journal of chemical physics* **1983**, *79*, 926–935.

(92) Case, D. A.; Babin, V.; Berryman, J.; Betz, R.; Cai, Q.; Cerutti, D.; Cheatham Iii, T.; Darden, T.; Duke, R.; Gohlke, H., et al. Amber 14. **2014**,

(93) Gotz, A. W.; Williamson, M. J.; Xu, D.; Poole, D.; Le Grand, S.; Walker, R. C. Routine microsecond molecular dynamics simulations with AMBER on GPUs. 1. Generalized born. *Journal of chemical theory and computation* **2012**, *8*, 1542–1555.

(94) Salomon-Ferrer, R.; Gotz, A. W.; Poole, D.; Le Grand, S.; Walker, R. C. Routine microsecond molecular dynamics simulations with AMBER on GPUs. 2. Explicit solvent particle mesh Ewald. *Journal of chemical theory and computation* **2013**, *9*, 3878–3888.

(95) Le Grand, S.; Götz, A. W.; Walker, R. C. SPFP: Speed without compromise—A mixed precision model for GPU accelerated molecular dynamics simulations. *Computer Physics Communications* **2013**, *184*, 374–380.

(96) Maier, J. A.; Martinez, C.; Kasavajhala, K.; Wickstrom, L.; Hauser, K. E.; Simmerling, C. ff14SB: Improving the Accuracy of Protein Side Chain and Backbone Parameters from ff99SB. *Journal of Chemical Theory and Computation* **2015**, *11*, 3696–3713.

(97) Berendsen, H. J. C.; Postma, J. P. M.; van Gunsteren, W. F.; DiNola, A.; Haak, J. R. Molecular dynamics with coupling to an external bath. *The Journal of Chemical Physics* **1984**, *81*, 3684–3690.

(98) York, D. M.; Darden, T. A.; Pedersen, L. G. The effect of long-range electrostatic interactions in simulations of macromolecular crystals: A comparison of the Ewald and truncated list methods. *The Journal of Chemical Physics* **1993**, *99*, 8345–8348.

(99) Kräutler, V.; Gunsteren, W. F. v.; Hünenberger, P. H. A fast SHAKE algorithm to solve distance constraint equations for small molecules in molecular dynamics simulations. *Journal of Computational Chemistry* **2001**, *22*, 501–508.

(100) Bowman, G. R.; Ensign, D. L.; Pande, V. S. Enhanced Modeling via Network Theory: Adaptive Sampling of Markov State Models. *Journal of Chemical Theory and Computation* **2010**, *6*, 787–794.

(101) Kohlhoff, K. J.; Shukla, D.; Lawrenz, M.; Bowman, G. R.; Konerding, D. E.; Belov, D.; Altman, R. B.; Pande, V. S. Cloud-based simulations on Google Exacycle reveal ligand modulation of GPCR activation pathways. *Nature Chemistry* **2014**, *6*, 15–21.

(102) Sculley, D. Web-scale k-means clustering. Proceedings of the 19th international conference on World wide web - WWW '10. Raleigh, North Carolina, USA, 2010; p 1177.

(103) Roe, D. R.; Cheatham, T. E. PTRAJ and CPPTRAJ: Software for Processing and Analysis of Molecular Dynamics Trajectory Data. *Journal of Chemical Theory and Computation* **2013**, *9*, 3084–3095.

(104) McGibbon, R.; Beauchamp, K.; Harrigan, M.; Klein, C.; Swails, J.; Hernández, C.; Schwantes, C.; Wang, L.-P.; Lane, T.; Pande, V. MDTraj: A Modern Open Library for the Analysis of Molecular Dynamics Trajectories. *Biophysical Journal* **2015**, *109*, 1528–1532.

(105) Scherer, M. K.; Trendelkamp-Schroer, B.; Paul, F.; Pérez-Hernández, G.; Hoffmann, M.; Plattner, N.; Wehmeyer, C.; Prinz, J.-H.; Noé, F. PyEMMA 2: A Software Package for Estimation, Validation, and Analysis of Markov Models. *Journal of Chemical Theory and Computation* **2015**, *11*, 5525–5542.

(106) Prinz, J.-H.; Wu, H.; Sarich, M.; Keller, B.; Senne, M.; Held, M.; Chodera, J. D.; Schütte, C.; Noé, F. Markov models of molecular kinetics: Generation and validation. *The Journal of chemical physics* **2011**, *134*, 174105.

(107) Metzner, P.; Schütte, C.; Vanden-Eijnden, E. Transition Path Theory for Markov Jump Processes. *Multiscale Modeling & Simulation* **2009**, *7*, 1192–1219.

(108) Humphrey, W.; Dalke, A.; Schulten, K. VMD: Visual molecular dynamics. *Journal of Molecular Graphics* **1996**, *14*, 33–38.

(109) Smart, O. S.; Neduvelil, J. G.; Wang, X.; Wallace, B. A.; Sansom, M. S. P. HOLE: A program for the analysis of the pore dimensions of ion channel structural models. *Journal of Molecular Graphics* **1996**, *14*, 354–360.

(110) Ramamoorthy, S.; Bauman, A. L.; Moore, K. R.; Han, H.; Yang-Feng, T.; Chang, A. S.; Ganapathy, V.; Blakely, R. D. Antidepressant-and cocaine-sensitive human serotonin transporter: molecular cloning, expression, and chromosomal localization. *Proceedings of the National Academy of Sciences* **1993**, *90*, 2542–2546.